

**This is the preprint version of the contribution published as:**

**Qian, L., Georgi, A., Gonzalez-Olmos, R., Kopinke, F.-D. (2020):**

Degradation of perfluorooctanoic acid adsorbed on Fe-zeolites with molecular oxygen as oxidant under UV-A irradiation

*Appl. Catal. B-Environ.* **278**, art. 119283

**The publisher's version is available at:**

<http://dx.doi.org/10.1016/j.apcatb.2020.119283>

# Degradation of perfluorooctanoic acid adsorbed on Fe-zeolites with molecular oxygen as oxidant under UV-A irradiation

*Lin Qian<sup>a</sup>, Anett Georgi<sup>\*a</sup>, Rafael Gonzalez-Olmos<sup>b</sup> and Frank-Dieter Kopinke<sup>a</sup>*

<sup>a</sup> Helmholtz Centre for Environmental Research – UFZ, Department of Environmental  
Engineering, Permoserstrasse 15, D-04318 Leipzig, Germany

<sup>b</sup> IQS School of Engineering, Universitat Ramon Llull, Via Augusta 390, 08017 Barcelona, Spain

## Abstract

Perfluorooctanoic acid (PFOA) is of emerging concern owing to its global distribution and environmental persistence. Efficient degradation approaches are so far limited. Herein, we demonstrate for the first time the photochemical degradation of PFOA under UV-A irradiation after adsorption on Fe-doped zeolites with molecular oxygen as the terminal oxidant. In a system containing 1 g L<sup>-1</sup> PFOA-loaded Fe-zeolites, outstanding PFOA decomposition (> 99%) was achieved within 24 h under slightly acidic conditions (pH ≤ 5.5). Short-chain perfluorinated carboxylic acids (PFCAs) are the main intermediates, beside fluoride and CO<sub>2</sub>. No PFOA degradation occurs with Fe-free zeolites or dissolved ferric ions. Furthermore, we investigated the effects of pH, inorganic ions and gas atmospheres on PFOA degradation. A photochemical degradation mechanism with zeolite-bound iron species as catalytic sites for carboxylate-to-metal charge transfer is proposed. The presented study offers a novel approach for the removal of the highly recalcitrant PFOA from contaminated waters.

**Keywords:** Fe-zeolites; Degradation; UV-A; Heterogeneous photochemistry; Perfluorooctanoic acid

## 1. Introduction

Perfluorooctanoic acid (PFOA) is one of the most important perfluorinated organic compounds: it possesses unique physicochemical properties and has been widely used in industrial and consumer applications [1-3]. Recently, PFOA has received much attention because it is extremely persistent in the environment and is detected in groundwaters [4], sediments [5] and human beings worldwide [6]. In addition, PFOA is resistant to most conventional reduction and oxidation

processes as well as biological degradation, due to the strong C-F bond [7-9]. It is practically inert to hydroxyl radicals ( $\bullet\text{OH}$ ) as it does not contain C-H bonds available for H abstraction [10].

Extensive research within the last two decades identified various reductive and oxidative pathways for PFOA degradation which in general require long reaction times and/or harsh conditions [11]. Reductive defluorination of PFOA requires solvated electrons that can be generated e.g. from the UV photolysis of iodide [12]. With respect to PFOA oxidation, it has been reported that electrochemical and photocatalytic treatments are efficient tools for degrading PFOA [13, 14]. Zhuo et al. used a Ti/SnO<sub>2</sub>-Sb-Bi electrode for electrochemical decomposition of PFOA and claimed that the oxidation of PFOA was initiated through a direct one-electron transfer from the carboxylate group to the anode [15]. Li et al. used indium oxide for the photocatalytic degradation of PFOA, where PFOA is decomposed directly by photogenerated holes of indium oxide under UV-C irradiation [16]. Alternatively, sulfate radicals produced by the thermolysis or photolysis of peroxydisulfate ( $\text{S}_2\text{O}_8^{2-}$ ) can decompose PFOA via the electron transfer from its carboxylate group to the sulfate radical [17, 18]. However, the efficiency of persulfates is rather low because the second-order rate constant for the reaction between sulfate radicals and PFOA ( $k_{\text{SO}_4\bullet} = (1.7\text{-}4.4) \times 10^4 \text{ M}^{-1}\text{s}^{-1}$ ) is much lower than those for typical water matrix components (e.g. chloride or carbonate) [19].

PFOA itself can hardly be degraded by direct photolysis, as it has a very weak light absorbance in the UV range [20, 21]. Nevertheless, by adding a certain amount of ferric ions to the system under acidic conditions ( $\text{pH} \leq 3.0$ ), PFOA degradation is promoted. It has been suggested that under these conditions  $[\text{PFOA-Fe}]^{2+}$  complexes are formed (reaction 1) and react under vacuum UV (V-UV, 185 nm) or UV-C (254 nm) irradiation to produce ferrous ions and carboxyl radicals via a ligand-to-metal charge transfer (reaction 2) [20, 22, 23]:



Decarboxylation of  $\text{C}_7\text{F}_{15}\text{COO}\cdot$  yields perfluorinated alkyl radicals  $\text{C}_7\text{F}_{15}\cdot$ . They may combine with molecular oxygen or hydroxyl radicals, or react with water to be decomposed further [24, 25]. In the presence of oxygen, ferrous ion can be re-oxidized to ferric ion, thus closing the catalytic iron cycle [23].

However, light with longer wavelength is unable to trigger such a ligand-to-metal charge transfer. Furthermore, the restricted operation pH range ( $\text{pH} \leq 3.0$ ), low reaction rates and the production of iron sludge in this homogeneous photochemical system will limit its applications in practical wastewater treatment.

Although the principle of ligand-to-metal charge transfer is known for PFOA degradation in solution, it has not been tested and reported in a heterogeneous system. In the present study, we found out that by adding Fe-loaded zeolites instead of aqueous ferric ions, the photochemical degradation of PFOA can already occur under UV-A irradiation ( $300 \text{ nm} < \lambda < 400 \text{ nm}$ ) instead of UV-C (e.g. at  $\lambda \approx 254 \text{ nm}$ ). Furthermore, as the zeolite acts as adsorbent for PFOA, a combination of adsorptive enrichment and photochemical degradation can be achieved. The separable heterogeneous catalyst and adsorbent can be used to concentrate PFOA from typical trace level polluted water streams and facilitates degradation under well-controllable conditions. These potential advantages are significant for application and justify a detailed mechanistic and optimization study.

Zeolites can be loaded with iron ions by simple ion exchange procedures. It has been shown in several studies that Fe-loaded zeolites are active as heterogeneous Fenton-like catalysts for the degradation of various organic contaminants by hydrogen peroxide [26, 27]. Isolated mononuclear

and binuclear iron species attached to acidic sites at the inner zeolite surfaces are generally attributed to high redox reactivity [28, 29]. In addition, Gonzalez-Olmos et al. observed an acceleration of dissolved organic carbon (DOC) removal in phenol degradation using Fe-loaded zeolites as catalysts, and ascribed this effect to a photo-Fenton reaction at the iron sites inside the zeolite pores improving the degradation of carboxylic acid intermediates [30].

The present study makes use of specific colloidal  $\mu\text{m}$ -sized Fe-zeolites: Trap-Ox<sup>®</sup>, a material designed for groundwater treatment [31]. The applied synthetic zeolites are of BEA framework type and were selected based upon an initial screening of PFOA adsorption to various zeolite types. Degradation of PFOA adsorbed to the Fe-zeolite under UV-A irradiation yields short-chain PFCAs as intermediates. Complete mass balances were obtained by means of an exhaustive extraction approach. The effects of pH, inorganic ions and gas atmospheres were investigated. Moreover, a degradation mechanism with molecular oxygen ( $\text{O}_2$ ) as the final oxidant is proposed.

## **2. Experimental Section**

### **2.1. Chemicals and Materials.**

All chemicals were in reagent grade and used without further purification, where not otherwise stated. Deionized water was used for the preparation of all solutions and suspensions. The Trap-Ox<sup>®</sup> zeolites BEA35 and Fe-BEA35 were provided by Clariant Produkte GmbH (Germany) and INTRAPORE GmbH (Germany), respectively. The number 35 represents the molar ratio of  $\text{SiO}_2/\text{Al}_2\text{O}_3$  for both zeolites. The BEA framework type is characterized by channels with 12 T atoms (T = Si or Al) having diameters of around 6.6-6.7 Å for the larger straight channels and 5.6-5.7 Å for the smaller zig-zag channels [32, 33]. Iron(III) oxide nanopowder (<50 nm particle size), PFOA ( $\text{C}_7\text{F}_{15}\text{COOH}$ , 96% purity) and heptafluorobutyric acid (HFBA,  $\text{C}_3\text{F}_7\text{COOH}$ , 98% purity)

were obtained from Sigma Aldrich. Perfluorohexanoic acid (PFHeA, C<sub>5</sub>F<sub>11</sub>COOH, 98% purity), perfluoropentanoic acid (PFPeA, C<sub>4</sub>F<sub>9</sub>COOH, 97% purity) and perfluoropropionic acid (PFPrA, C<sub>2</sub>F<sub>5</sub>COOH, 97% purity) were obtained from J&K Scientific. Perfluoroheptanoic acid (PFHpA, C<sub>6</sub>F<sub>13</sub>COOH, 97% purity) was obtained from Alfa Aesar. Trifluoroacetic acid (TFA, CF<sub>3</sub>COOH, 99% purity) was obtained from Fluka.

## **2.2. Catalyst Pre-treatment.**

In this study, commercially available Fe-BEA35 was used as adsorbent and catalyst. Preliminary experiments showed that the original Fe-BEA35 contains a certain amount of labile iron which is potentially leached during the reaction. Therefore, a pretreatment procedure was applied in order to stabilize iron as Fe<sup>3+</sup> and remove any leachable iron by competitive exchange with potassium ions under acidic conditions [34]: 4 g of Fe-BEA35 in a 50 mL plastic centrifuge vial was mixed with 40 mL of 0.1 M KNO<sub>3</sub> (pH = 3.0) and 100 μL of 30 wt-% H<sub>2</sub>O<sub>2</sub> solution. The suspension was shaken overnight, centrifuged at 2500 rpm for 5 min and the supernatant was removed. This washing procedure was repeated a second time (2 h contact), after which the solid was washed twice with 20 mL deionized water (1 h contact). Finally, the Fe-BEA35 was dried in an oven at 80 °C.

## **2.3. Photochemical Procedures and Reusability Test.**

Where not otherwise stated, an aqueous PFOA solution (100 mL, 48 μM) was mixed with 0.1 g of Fe-BEA35 in a 200 mL glass bottle followed by shaking for 24 h in order to obtain a homogeneous suspension. The calculated concentrations of total iron in Fe-BEA35 and PFOA under these conditions are  $2.32 \times 10^{-4}$  M and  $4.83 \times 10^{-5}$  M, respectively. In one set of experiments,

the PFOA concentration was increased by a factor of 10. 0.1 M HCl and 0.1 M NaOH were used to adjust pH values. 30 mL suspension was taken to a 40 mL quartz bottle equipped with a Mininert<sup>TM</sup> valve. The suspension was purged with oxygen or nitrogen gas for 10 min shortly before UV irradiation. The quartz bottle was shaken during the degradation process with 240 rpm to ensure a good dispersion of the zeolite particles (see Figure S1, Supporting Information (SI)). The reactions under nitrogen atmosphere were performed in a nitrogen-filled glovebox in order to preclude penetration of oxygen into the reaction vessels. For irradiation, a mercury lamp (either 4 W, UV-A, central wavelength 365 nm, or 4 W, UV-C, central wavelengths 254 nm, both from Herolab GmbH Laborgeräte, Germany) was placed beneath the plane reactor basal face, which was made from quartz glass. The photon flux was determined by means of ferrioxalate actinometry to be  $4.47 \times 10^{-6} \text{ mol s}^{-1}$  under UV-A and  $4.54 \times 10^{-6} \text{ mol s}^{-1}$  under UV-C, respectively. The spectral curves of these two UV lamps are shown in Figure S2. The distance between the UV lamp screen and the bottom of the reactor was 20 mm. Details of the reactor setup are shown in Figure S1.

Samples of the reaction suspension were taken at certain time intervals. In order to determine the total amounts of PFOA and byproducts (including adsorbed fractions), an exhaustive extraction approach was used as follows: 100  $\mu\text{L}$  aliquots of suspension were taken and sulfuric acid was used to adjust the suspension to pH 2, and then extracted with 2 mL acetonitrile for 24 h. The suspension was centrifuged at 2500 rpm for 5 min, and the clear supernatant was taken for LC-MS analysis. The applied extraction method was developed in preliminary tests where acetonitrile extraction at various pH values was studied. Acidic conditions showed the highest PFOA recovery. Fluoride and the freely dissolved acid concentrations in the aqueous phase were determined by IC

and LC-MS analysis, using the clear supernatants obtained by centrifugation of 1 mL suspension aliquots (2500 rpm for 5 min).

UV-A irradiation leads to degradation of PFOA into short-chain PFCAs which are released into the aqueous phase thus regenerating the adsorbent. For a complete mineralization of these degradation products, the aqueous phase of the suspension in one experiment was subsequently treated by UV-C activation of sodium persulfate as follows: the UV-A irradiated suspension was centrifuged at 2500 rpm for 5 min to separate the zeolite particles which were practically free of residual PFCAs. The clear supernatant was taken and 8.4 mM sodium persulfate was added once every 2 hours, followed by UV-C irradiation until all of the short-chain PFCAs were decomposed.

For catalyst reusability tests ( $1 \text{ g L}^{-1}$  Fe-BEA35,  $C_{0,\text{PFOA}} = 48 \text{ }\mu\text{M}$ ,  $\text{pH}_0 = 5.5$ , oxygen purged), after every irradiation period the supernatant was removed and replaced by the same volume of fresh aqueous PFOA solution. After shaking for 1 day for adsorption equilibration, the suspension was ready for the next irradiation run.

#### **2.4. Analysis.**

PFOA and its degradation products PFHpA (C7), PFHeA (C6), PFPeA (C5), and PFBA (C4) were measured by means of a HPLC system coupled to a single-stage quadrupole mass spectrometer with electrospray ionization (LCMS-2020; SHIMADZU Corp.). Aliquots of 3  $\mu\text{L}$  of the solution containing the target compounds were injected by an auto-sampler into a 100 mm  $\times$  2 mm Gemini C6-Phenyl column (110 Å pore and 3  $\mu\text{m}$  particle size, Phenomenex) at 40 °C. The mobile phase was a combination of 30 vol-% solvent A (10 mM ammonium acetate dissolved in 90 vol-% deionized water and 10 vol-% methanol) and 70 vol-% solvent B (10 mM ammonium acetate dissolved in 90 vol-% methanol and 10 vol-% deionized water), delivered at a flow rate of 0.3 mL  $\text{min}^{-1}$  with a total run time of 33 min. The correlation coefficients ( $R^2$ ) of the calibration

curves for PFOA and the other acids were  $\geq 0.99$  for sample concentrations  $\leq 1 \text{ mg L}^{-1}$ . PFPrA (C3), TFA (C2). Fluoride concentrations were analyzed by means of an IC DX 500 ion chromatograph (Dionex) equipped with an anion suppressor (ASRS300), conductivity detector (IC 25) and an IonPac AS11-HC column (250 mm  $\times$  4 mm) using a flow rate of  $1 \text{ mL min}^{-1}$  and the following eluent gradient: 1 mM KOH from 0 to 8 min, increased linearly to 30 mM KOH over 20 min and held at 30 mM KOH for 2 min. In this study, the defluorination ratio ( $d_{F^-}$ ) is calculated as follows:

$$d_{F^-} = \frac{C_F}{15 \times C_0} \times 100\% \quad (3)$$

where  $C_F$  is the fluoride concentration ( $\mu\text{M}$ ) and  $C_0$  is the initial concentration of PFOA ( $\mu\text{M}$ ). The factor 15 represents the number of fluorine atoms in one PFOA molecule. Complete defluorination of PFOA results in  $d_{F^-} = 100\%$ .

The analysis of gas phase intermediates was conducted on a GC/MS (GCMS-QP2010, SHIMADZU Corp.) by means of headspace sampling (25  $\mu\text{L}$  gas) after 24 h irradiation. The GC separation column was a 30 m DB1 (0.32 mm inner diameter, 0.25  $\mu\text{m}$  film thickness). The MS was operated in the SCAN-mode ( $m/z = 41\text{-}500$  amu). The injector temperature was set at  $150 \text{ }^\circ\text{C}$ , and the GC oven program was isothermal at  $35 \text{ }^\circ\text{C}$ .

A Zetasizer Nano ZS (Malvern Instruments Ltd, U.K.) was used for dynamic light scattering (DLS) and zeta potential measurements. Scanning electron microscopy images were recorded with a Zeiss Merlin VP scanning electron microscope (Zeiss, Germany). X-ray photoelectron spectroscopy (XPS) measurements were performed on an Axis Ultra photoelectron spectrometer (Kratos, Manchester, UK) using monochromatized Al  $K\alpha$  radiation ( $h\nu = 1486.6 \text{ eV}$ ). X-ray powder diffraction (XRD) patterns were obtained on a Bruker D8-Advance diffractometer. For details of XPS and XRD measurements see SI part.

UV–vis diffuse reflectance spectra (DRS) of zeolite samples were obtained for the 10 g L<sup>-1</sup> zeolite suspensions using a Varian Cary 3 spectrophotometer with a diffuse reflectance accessory in the 190–600 nm range. BaSO<sub>4</sub> powder was used as a non-absorbing reference standard. The spectra were converted according to the Kubelka–Munk function and deconvoluted into sub-bands with Gaussian peak shape using Origin 2018 [31]. Spectra were interpreted by comparing the positions of the resulting peaks with literature data [31, 35, 36].

### **3. Results and Discussion**

#### **3.1. Catalyst characterization**

As shown in Figure 1, Fe-BEA35 zeolites comprise joined spherical particles without sharp edges. According to the SEM images, the diameter of primary particles is around 0.5 μm. Table S1 shows the particle size distribution of Fe-BEA35 in suspension, which was determined by means of dynamic light scattering revealing a mean diameter of 0.86 μm. It was in good accordance with the particle size determined by laser diffraction for the dry Fe-BEA35 powder samples. The XRD pattern was in good agreement with the BEA framework type as shown in Figure S3 [37]. The iron content of the Fe-BEA35 was measured to be 1.3 wt-% by X-ray fluorescence analysis. In addition, the peak at binding energy of 711.2 eV in Fe 2p 3/2 XPS spectra of Fe-BEA35 indicates the existence of Iron (III) (Figure S4) [38]. A BET surface area of 600 m<sup>2</sup> g<sup>-1</sup> and a total pore volume of 0.42 cm<sup>3</sup> g<sup>-1</sup> were determined from N<sub>2</sub> adsorption/desorption measurements (for details see SI part).

#### **3.2. Photochemical degradation of PFOA in the presence of Fe-BEA35 under UV-A irradiation.**

From the point of view of application, UV-A has a number of advantages over shorter wavelengths, including potential use of solar irradiation or LEDs and less demands on material selection for reactor design. A typical reaction suspension contained  $1 \text{ g L}^{-1}$  Fe-BEA35 and  $C_{0,\text{PFOA}} = 48 \text{ }\mu\text{M}$  with  $\text{pH}_0 = 5.5$ . Under these conditions, PFOA was predominantly in the adsorbed state, as only 16% of the initially added PFOA was detected in the aqueous phase after the pre-equilibration period of 24 h, i.e. before start of the irradiation period. Thus, the initial loading of PFOA on the zeolite was  $16.8 \text{ mg g}^{-1}$ . In order to follow the total concentrations, residual PFOA and intermediates were extracted from the zeolite into the liquid phase by adding sulfuric acid to adjust pH to 2, and then introducing 95 vol% acetonitrile for extraction. The recovery of PFOA in this procedure (before irradiation) was nearly complete, i.e.  $(94 \pm 3)\%$ .

In order to elucidate the photochemical degradation mechanism, control experiments were carried out under the same conditions in the presence of non-Fe-doped BEA35 and in the absence of zeolite but presence of ferric ions ( $\text{pH}_0 = 3.0$  and  $5.5$ , Figure 2(a)). As revealed by previous studies, PFOA has almost no absorption in the UV-A range and the direct photolysis of PFOA does not take place in relevant time scales [20, 21]. In addition, PFOA degradation within 24 h is also insignificant in the presence of  $200 \text{ }\mu\text{M Fe}^{\text{III}}$  at  $\text{pH} = 3.0$  (dissolved Fe) and  $5.5$  (colloidal Fe) under UV-A irradiation, as indicated by the two control experiments. No PFOA degradation was also observed with BEA35 (no iron). However, in the presence of Fe-BEA35, up to 90% of the initial PFOA was decomposed after 6 h of UV-A irradiation, and complete degradation ( $> 99\%$ ) with  $d_{F^-} = 38\%$  was achieved within 24 h. When applying a high-surface area iron oxide, i.e. iron (III) oxide nanoparticles (Figure S5), almost no PFOA degradation was observed within 24 h. Thus, only the combination of UV-A irradiation and Fe-BEA35 effected a significant PFOA degradation and the Fe speciation within the zeolite obviously plays an important role.

In spite of its almost complete degradation, only a partial defluorination of PFOA was achieved within 24 h. We found six shorter-chain perfluorinated carboxylic acids (PFCAs) with 2 to 7 carbon atoms. They were identified and quantified by LC/MS (C7 to C4) and IC (C3 and C2) analysis. Their concentration time profiles, shown in Figure 2(b), indicate that the longer-chain PFCAs are decomposed stepwise towards shorter-chain PFCAs during the irradiation. The possible reason for steadily increasing concentrations of C5 to C2 PFCAs was further investigated by means of adsorption experiments.

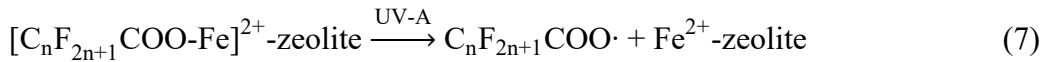
$X_{\text{sorb}}$  and  $X_{\text{free}}$  as the fractions of adsorbed and freely dissolved PFCA, respectively, were calculated according to eqs. 4 and 5, where  $C_{\text{PFCA,free}}$  and  $C_{\text{PFCA,total}}$  are the freely dissolved and total PFCA concentrations added, respectively.

$$X_{\text{sorb}} = 1 - X_{\text{free}} \quad (4)$$

$$X_{\text{free}} = C_{\text{PFCA,free}} / C_{\text{PFCA,total}} \quad (5)$$

As shown in Figure 3,  $X_{\text{sorb}}$  decreases with decreasing chain lengths, e.g. the distribution between  $X_{\text{sorb}}$  and  $X_{\text{free}}$  in 1 g L<sup>-1</sup> zeolite suspensions changes from 84:16 for PFOA to 10:90 for PFBA. This may explain why the shorter-chain PFCAs are accumulated in irradiated zeolite suspensions: they are preferably released from the zeolite phase where the photochemical reaction takes place.

It can be hypothesized that complex formation is a pre-requisite for photochemical degradation of PFCAs according to eqs. 6 and 7:



Based on this mechanism, a simplified rate equation (8) can be derived:

$$\frac{d[\text{PFCA}]}{dt} = -k \cdot C_{[\text{C}_n\text{F}_{2n+1}\text{COO-Fe}]^{2+}\text{-zeolite}} = -k \cdot X_{\text{complex}} \cdot C_{\text{PFCA, total}} \quad (8)$$

where  $X_{\text{complex}}$  (with  $0 \leq X \leq 1$ ) is the fraction of PFCA in reactive complexes. To better illustrate the PFCAs complex formation, a schematic diagram of PFOA adsorbed on Fe-BEA35 was displayed in Figure 4. Two adsorptive states of PFOA are presented on the zeolite: complexed PFOA (i.e. specifically adsorbed PFOA at ferric ions) and non-specifically adsorbed PFOA. The complexed PFOA is signified by its carboxylic group in the close vicinity to the ferric ions, which enables the carboxylate-to-metal charge transfer upon irradiation, while the non-specifically adsorbed PFOA has less or no chance to allow the charge transfer as its carboxylic group is not able to reach the ferric ions. While  $X_{\text{complex}}$  cannot be easily determined, the overall degree of adsorption ( $X_{\text{sorb}}$ ) is obtained experimentally (eqs. 4 and 5). Thus, using lumped rate coefficients  $k'$  and  $k''$

$$k' = k \cdot X_{\text{complex}}/X_{\text{sorb}} \quad (9)$$

$$k'' = k' \cdot X_{\text{sorb}} \quad (10)$$

eq. 8 can be simplified to a pseudo-first-order rate law:

$$\frac{d[\text{PFCA}]}{dt} = -k' \cdot X_{\text{sorb}} \cdot C_{\text{PFCA, total}} = -k'' \cdot C_{\text{PFCA, total}} \quad (11)$$

The  $X$  values and the ratio  $X_{\text{complex}}/X_{\text{sorb}}$  are related to compound properties such as chain lengths of PFCAs, which determine their hydrophobicity and thus their tendency for non-specific adsorption into the zeolite. The composition of the aqueous phase, e.g. pH value and concentrations of competing inorganic ions as well as other factors, can also affect  $X_{\text{complex}}/X_{\text{sorb}}$ , which will be discussed in the following chapters. In addition, it is worth noting that pseudo-first-order kinetics cannot describe the whole degradation curve according to the experiment, but gives satisfying fitting within the initial reaction period (0 – 6 h) (Figure S6).

The fluorine mass balance during Fe-zeolite-catalyzed photo-degradation of PFOA is shown in Figure 2(c). The fluorine in the suspension is grouped into four contributions: the remaining

PFOA, C5 to C7 PFCAs, C2 to C4 PFCAs and fluoride. The initial recovery by acetonitrile extraction is around  $(94 \pm 3)\%$  after 24 h adsorption. The final recovery of fluorine in the form of the various products related to total PFOA initially added is  $(89 \pm 5)\%$  after 24 h of irradiation. Some highly volatile fluorinated alkanes, i.e.  $C_nHF_{2n+1}$  were formed as detected by GC/MS headspace analysis (see Table S2) but only in trace amounts ( $<0.1$  mol-% of initial PFOA).

It should be pointed out that the remaining shorter-chain products desorb from the zeolite and accumulate in the aqueous phase. Thus, the process can be exploited in terms of regeneration of the adsorbent for PFOA adsorption. Comparing with PFOA, the toxicity of these shorter-chain products is lower [39-41]. Nevertheless, the aqueous phase containing shorter-chain products is a concentrated regeneration solution which can be subject to further degradation, e.g. by oxidation with sulfate radicals produced from UV activation of persulfate [17, 19]. To test whether a complete mineralization of PFOA by a UV/persulfate post-treatment of the regeneration solution is feasible, the aqueous phase of the 24 h-UV-A irradiated PFOA/zeolite suspension was further treated by UV-C activation in the presence of sodium persulfate. A certain amount of sodium persulfate was added portion-wise every two hours to minimize the self-scavenging effect otherwise would occur when a large amount of sodium persulfate is added at a time. As shown in Figure S7, the shorter-chain PFCAs (C2, C3, C4, C5 and C6) were nearly completely decomposed within 10 h. Thus, a nearly complete defluorination ( $86 \pm 4\%$ ) and mineralization of PFOA was achieved by the combined process (Figure S8). It is worth noting that the degradation of PFCAs by sulfate radicals is strongly suppressed by typical water matrix components such as chloride [19]. Thus, it is obvious that for future design of a technical process, the sequence of steps is the key to improved efficiency, i.e. I) PFOA adsorption out of e.g. contaminated groundwater into zeolite particles, II) separation of particles and III) PFOA photodegradation inside the zeolite releasing

shorter-chain acids into a controllable regeneration solution (water largely free of chloride, carbonate and natural organic matter as typical radical scavengers) which can be IV) post-treated by UV/persulfate.

### **3.3. Effect of the adsorption of PFCAs on the photochemical degradation of PFOA.**

One of the driving forces of PFCAs adsorption on zeolites is the hydrophobic effect, as the hydrophobic perfluoroalkyl chains of PFCAs find a suitable environment in the narrow zeolite channels. The electrostatic repulsion between terminal aluminol groups (internal surface) and silanol groups (external surface) of Fe-BEA35 and carboxylate head groups of PFCAs counteracts the adsorption [42]. As the Al content in the zeolite is low (1 Al atom per 17 Si atoms) it can be assumed that zeolite-bound  $\text{Fe}^{3+}$  ions cannot be coordinatively saturated by sufficient negatively charged aluminol groups in close proximity but need further ligands, e.g.  $\text{OH}^-$  or  $\text{H}_2\text{O}$  and can also bind PFCA anions. As can be seen from Figure 3, adsorption affinity of PFCAs decreases with decreasing chain length and thus decreasing hydrophobicity. Thus, the complexing ability of the zeolite-bound  $\text{Fe}^{3+}$  for PFCAs is obviously not strong, instead one can assume a synergistic effect of electrostatic interactions between  $\text{R-COO}^-$  and  $\text{Fe}^{3+}$  sites together with hydrophobic interactions of the perfluoroalkyl chain in the zeolite channels.

It is considered that the performance of the photochemical degradation of PFCAs is dependent on two steps: i) the adsorption of PFCAs into the zeolites, and ii) the formation of the complex between PFCAs and ferric ions. Since the  $\text{p}K_a$  values of the C2 and C8 PFCAs are comparably low, i.e. close to 0 [43], it is reasonable to speculate that the complexing abilities should not differ greatly in the series of PFCAs. The effect on the photochemical degradation of PFCAs caused by different complexing abilities of PFCAs can thus be neglected.

In order to understand the impact of adsorption on the photochemical degradation of PFCAs, the degradation of PFOA and PFBA as PFCAs with different perfluoroalkyl chain lengths, was investigated and compared in Figure 5. By fitting the degradation curves using pseudo-first-order kinetics in accordance with eq. 11, it was found that  $k_{\text{obs,PFOA}}$  is by a factor of 10 higher than  $k_{\text{obs,PFBA}}$ . This is in line with a factor of 8.4 in  $X_{\text{sorb}}$  for PFOA compared to PFBA. Thus, it can be concluded that the hydrophobic interactions provided by the zeolite channels for the perfluoroalkyl chains of PFCAs play an important role in the iron-catalyzed photodegradation process. Indeed, a lower  $X_{\text{sorb}}$  value indicates a smaller possibility of PFBA to be adsorbed and complexed, resulting in an accumulation of PFBA up to the end of the 24 h irradiation time (Figure 2(b)).

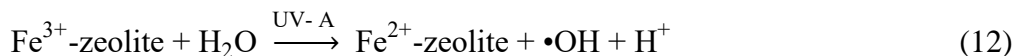
### 3.4. Effect of pH on the photochemical degradation of PFOA.

Figure 6(a) and (b) show the degradation and defluorination behaviors of PFOA within 24 h UV-A irradiation at various initial pH conditions. The distribution of PFOA between zeolite and aqueous solution at various initial pH values is shown in Table 1. The zeta potential of Fe-BEA35 at different pH values is shown in Table S3. The zeta potential of Fe-BEA35 becomes more negative with increasing pH values. However, it should be noticed that zeta potential reflects the charge at the external particle surface only whereas the inner surfaces provide the highest contribution to specific surface area and adsorption. The initially adsorbed fractions of PFOA ( $X_{\text{sorb}}$ ) on Fe-BEA35 are 98% and 84% at pH 3.0 and 5.5, respectively. The extents of PFOA degradation and the corresponding  $d_{F^-}$  are identical for the reactions under these acidic conditions ( $\text{pH}_0 = 3.0$  or 5.5). However, under neutral and alkaline conditions ( $\text{pH}_0 = 7.0$  and 9.0), PFOA degradation is significantly inhibited, although about 70% is still in an adsorbed state (Table 1). More precisely, increasing pH from 5.5 to 7.0 and 9.0 results in only 16% and 18% reduction in  $X_{\text{sorb}}$  but in 21 and 35 times higher PFOA half-life, respectively. This points to significant changes

in PFOA speciation within the zeolite when pH changes. When pH increases, though the majority of PFOA remains adsorbed, a fraction of complexed PFOA is likely shifted to non-specifically adsorbed sites as is shown in Figure 4. The possible reason for this PFOA speciation variation is the change of ligand environment within the zeolite when pH is increasing. The ferric ions can complex with other ions, e.g. they have a strong affinity to hydroxide ions [44]. As a consequence of pH increasing, more hydroxide ions will compete with the complexed PFOA at the ferric ions and push the latter to non-specifically adsorption sites. Similar effect is assumed for the shorter chains PFCAs as well. In short, the negative influence of pH increasing on PFOA photochemical degradation is attributed to a lower fraction of complexed PFOA (PFOA-Fe<sup>3+</sup>) in favor of its non-specifically adsorbed fraction caused by a change in the ligand environment: replacement of H<sub>2</sub>O by OH<sup>-</sup> ligands at the iron. As mentioned in the previous section, the adsorption of PFOA on zeolites is a precondition, but the specific complexation between PFOA and ferric ions in the zeolite is the key factor for its photochemical degradation. Additionally, the pH value also influences the PFCAs adsorption. When the pH value decreases, the density of negative surface charges is reduced. The electrostatic repulsion between PFOA and zeolite becomes weaker, which promotes the adsorption. To sum up, acidic or slightly acidic conditions are optimal for this system.

### **3.5. Effect of inorganic ions and atmosphere on photochemical degradation of PFOA.**

The influence of four inorganic anions, i.e. sulfate (SO<sub>4</sub><sup>2-</sup>), nitrate (NO<sub>3</sub><sup>-</sup>), chloride (Cl<sup>-</sup>) and perchlorate (ClO<sub>4</sub><sup>-</sup>), on PFOA degradation is presented in Figure 7(a) and Table 2. Apart from SO<sub>4</sub><sup>2-</sup>, the addition of other anions has very limited or almost no influence on PFOA degradation kinetics and defluorination. Two possible effects can be considered as negative impacts: (i) competitive complexation with ferric ions;[44] and (ii) capture of hydroxyl radicals (•OH) which are formed by the photolysis of ferric species and water under UV-A irradiation (eq. 12) [45].



A significant inhibiting effect on PFOA degradation and defluorination is observed in the presence of  $\text{SO}_4^{2-}$ . In fact,  $\text{SO}_4^{2-}$  rarely reacts with  $\bullet\text{OH}$ , but it has the potential to coordinate with ferric ions in Fe-BEA35. The affinity for interaction between ferric ions and the anions follows the order of  $\text{OH}^- > \text{SO}_4^{2-} > \text{Cl}^- > \text{NO}_3^- > \text{ClO}_4^-$  [44]. As a consequence,  $\text{SO}_4^{2-}$  may interfere most strongly with the complexation between PFOA and ferric ions, and thus reduce  $k_{\text{obs,PFOA}}$  and  $d_{\text{F}^-}$ . The introduction of  $\text{Cl}^-$  has only a slight influence on  $k_{\text{obs,PFOA}}$  and  $d_{\text{F}^-}$ , which may also be caused by the competitive complexation of ferric ions. Alternatively,  $\text{Cl}^-$  will react with  $\bullet\text{OH}$ . Although  $\bullet\text{OH}$  itself cannot attack PFOA, it can promote the re-oxidation of ferrous ions and may be involved in the conversion of intermediates, thus playing a significant role during defluorination of PFOA. Nevertheless, the presence of  $\text{NO}_3^-$  and  $\text{ClO}_4^-$  has practically no negative effect on  $k_{\text{obs,PFOA}}$  and  $d_{\text{F}^-}$ , compared with the reference case where no salts were added.

In order to understand the mechanism of the photochemical degradation of PFOA better, the influence of dissolved oxygen on PFOA degradation and defluorination was investigated. Where not otherwise stated, reactions were conducted in closed vessels with a certain headspace volume of pure oxygen (10 mL  $\text{O}_2$  per 30 mL of aqueous phase). The system was not purged with oxygen continuously because the amount of oxygen (446  $\mu\text{mol}$ ) in the headspace was sufficient for accepting all electrons released in total mineralization of PFOA (1.45  $\mu\text{mol}$ ). When the reaction was carried out under nitrogen atmosphere, the photochemical degradation of PFOA was strongly inhibited (Table 2 and Figure 7(a)). The  $d_{\text{F}^-}$  after 24 h irradiation decreased from 38% to 12%, and the  $k_{\text{obs,PFOA}}$  decreased from 0.23  $\text{h}^{-1}$  to 0.040  $\text{h}^{-1}$ . The role of oxygen in photochemical degradation of PFOA becomes even more obvious when a 10 times higher initial PFOA concentration (480  $\mu\text{M}$ ) was introduced. As seen in Table S4 and Figure 7(b), the  $d_{\text{F}^-}$  after 48 h

irradiation time was 22.1% and 2.1%, and the  $k_{\text{obs,PFOA}}$  was  $0.046 \text{ h}^{-1}$  and  $0.0045 \text{ h}^{-1}$ , under oxygen and nitrogen atmospheres, respectively. These results clearly show that oxygen plays an important role in the photochemical degradation of PFOA. Molecular oxygen may be involved in at least three reactions: (i) it is the source for reactive species such as  $\bullet\text{OH}$  and  $\bullet\text{O}_2\text{H}$ , which may also promote the re-oxidation step as well as facilitate the mineralization of PFOA intermediates [25], (ii) it facilitates the re-oxidation of ferrous iron to ferric iron and thus closes the catalytic cycle as also discussed by Hori et al. [23], and (iii)  $\text{O}_2$  is directly involved in the complex radical chemistry of PFCA degradation (eq. (16)).

### **3.6. Photochemical properties of Fe-BEA35.**

In order to characterize the photochemical properties of Fe-BEA35, UV-vis-DRS values were measured. This technique is able to distinguish between different isolated iron species and iron oxide clusters. The spectra of Fe-BEA35 and BEA35 zeolites as well as the deconvolution of the spectrum of Fe-BEA35 are shown in Figure 8. The spectrum of Fe-BEA35 shows strong and broad absorption bands in the ultraviolet and visible range. Its deconvolution reveals five peaks. Based on literature sources [31, 35, 36], the absorption bands below 220 nm and around 280 nm are ascribed to  $\text{Fe}^{3+}$  ions in tetrahedral and octahedral coordination, respectively. The absorption band around 350 nm is ascribed to octahedral  $\text{Fe}^{3+}$  ions in small oligomeric iron oxide clusters. The absorption bands around 400 nm and above 450 nm are ascribed to larger iron-oxide particles. In various redox reactions catalyzed by Fe-zeolites, isolated iron sites are assumed to be more active than the iron oxide clusters [28]. In the present study, the photochemical degradation of PFOA on Fe-BEA zeolites takes place under UV-A irradiation. The overlap between the UV-A emission (320 to 380 nm, see Figure S2) and the absorption bands of isolated  $\text{Fe}^{3+}$  ions (especially those in octahedral coordination, 200 to 340 nm, see Figure 8) is in accordance with the hypothesis that

these sites are involved in the carboxylate-to-metal charge transfer ( $\text{Fe}^{3+} \leftarrow \text{O}$ ) under UV-A irradiation [36, 46]. Part of the adsorbed PFOA is assumed to be complexed with  $\text{Fe}^{3+}$  ions at such positions, so these PFOA- $\text{Fe}^{3+}$ -zeolite complexes can be excited by UV-A irradiation and finally decomposed by decarboxylation. The distribution of iron species shown by the deconvolution also fits to the observation presented in Figure 8: not all the iron species in Fe-BEA35 are active in photochemical degradation of PFOA. In the absence of dissolved oxygen (i.e. without recycling of ferric iron), only 24% of 480  $\mu\text{M}$  PFOA was converted after 48 h irradiation. This amount corresponds to 114  $\mu\text{M}$  redox-active  $\text{Fe}^{3+}$  species of approx. 232  $\mu\text{M}$  total iron content in 1 g  $\text{L}^{-1}$  Fe-BEA35. In other words, only about 50% of the  $\text{Fe}^{3+}$  present in the zeolite Fe-BEA35 is available as electron acceptor. Compared with Fe-BEA35, the UV-vis-DR spectrum of BEA35 exhibits no strong absorption bands, due to the absence of iron (Figure 8). In addition, we investigated the UV-vis-DR spectra of Fe-BEA35 with and without PFOA loading (Figure S9). Surprisingly, the two spectra are almost identical. As discussed above, the ferric ions have a strong affinity to hydroxide ions, so it can be speculated that only a small fraction of the adsorbed PFOA is actually in a complexed state. In this case, the absorption spectra of PFOA- $\text{Fe}^{3+}$  complexes cannot be well characterized by UV-vis-DRS.

According to the UV-vis-DR spectrum of Fe-BEA35, it may be possible to improve the photochemical efficiency by shifting the irradiation to shorter wavelengths. As is shown in Figure 9, the degradation and defluorination behavior of PFOA is considerably enhanced under UV-C irradiation with 254 nm. The  $d_{\text{F}^-}$  after 24 h under UV-C irradiation was increased from 38% to 49%, and the  $k_{\text{obs,PFOA}}$  increased from 0.38  $\text{h}^{-1}$  to 0.82  $\text{h}^{-1}$ . The improvement in photochemical degradation of PFOA is reasonable, because the absorption band around 280 nm, referring to  $\text{Fe}^{3+} \leftarrow \text{O}$  charge transfer in isolated  $\text{Fe}^{3+}$  ions, is the strongest sub-band. From the application point

of view, however, UV-A irradiation has significant advantages over UV-C irradiation with respect to reactor equipment and potential use of LED lamps or even natural sunlight. Further optimization potential for the Fe-BEA35 catalyst lies in decreasing the proportion of iron oxide clusters and large iron-oxide particles, because their absorption bands around 350 nm and 400 nm compete for photons from UV-A irradiation and thus decrease the photochemical efficiency of this redox-catalyst.

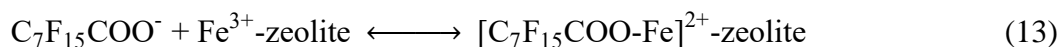
### **3.7. Reusability Test.**

Figure 10 shows degradation and defluorination behaviors of PFOA in a recycling experiment. The catalyst activity showed a slightly decreasing tendency, but maintained about 80% of its initial activity in the sixth consecutive run. Two reasons can be considered to explain the observed apparent decrease in catalytic performance: (i) unavoidable mass losses of the catalyst during the recycling process, and (ii) some carry-over of adsorbed PFOA and its reaction products between the runs. Neither phenomenon affects the inherent catalyst activity. These results demonstrate that Fe-BEA35 is relatively stable and has a promising potential for practical application.

### **3.8. Possible pathways of photochemical degradation of PFOA.**

Based on the presented results, a reaction mechanism is proposed in Scheme 1. It is similar to suggested schemes for PFOA photo-degradation in homogeneous iron-containing solutions from the literature [19, 20, 25, 47]. First, the adsorbed PFOA is complexed with isolated  $\text{Fe}^{3+}$  ions in tetrahedral and octahedral coordination to form PFOA- $\text{Fe}^{3+}$  complexes. After the excitation under UV-A irradiation, complexed PFOA is oxidized via a ligand-to-metal charge transfer process (eq. 14) [20, 22, 23]. The resulting carboxyl radicals decarboxylate, yielding perfluorinated alkyl radicals ( $\bullet\text{C}_7\text{F}_{15}$ ) (eq. 15) [48]. The  $\bullet\text{C}_7\text{F}_{15}$  can then react further, preferentially with dissolved oxygen (eq. 16). The subsequent radical and hydrolysis reactions are proposed in the literature [19,

47] but remain speculative (eqs. 18-22). In particular, radical-radical reactions such as (17) and (18) are less likely in the zeolite pores. The shorter-chain PFCAs follow a similar degradation pathway as PFOA. In order to close the photocatalytic cycle, reduced iron sites must be re-oxidized either by molecular oxygen or by •OH radicals (eqs. 23 and 24).



Perfluorinated alkyl radicals ( $\cdot\text{C}_n\text{F}_{2n+1}$ ) are key intermediates in the supposed reaction pathway. In the absence of dissolved oxygen (nitrogen atmosphere), they were expected to stabilize by bimolecular reactions such as recombination or disproportionation or by H-abstraction from water. Indeed, trace amounts of corresponding 1H-perfluoroalkanes ( $\text{C}_n\text{F}_{2n+1}\text{H}$ ) were detected in the gas phase as shown in Table S2. However, even in the presence of reactive H-donors such as methanol (1 vol-%),  $\text{C}_7\text{F}_{15}\text{H}$  was detected only at a trace level (<0.1 mol-% of converted PFOA). The corresponding experiments took carefully into account the volatility of these compounds.

Therefore, the supposed reaction mechanism in the absence of O<sub>2</sub> must be considered as a hypothesis requiring additional proof. Understanding the fate of perfluoroalkyl radicals is not only an academic question: reactions with O<sub>2</sub> and •OH (eqs. 16 and 17) result in shorter-chain PFCAs, which have to be chemically degraded further. Other radical stabilization reactions, such as H-abstraction from appropriate H-donors (or water), would produce highly volatile compounds (e.g. C<sub>n</sub>F<sub>2n+1</sub>H) which are easily removed from the aqueous phase. Hence, controlling the fate of the key intermediate •C<sub>n</sub>F<sub>2n+1</sub> would provide a tool to make the entire treatment process more efficient.

In addition, methanol can also work as an effective •OH quencher. As seen in Figure S10, the addition of methanol (1 vol-%) has almost no effect on PFOA degradation and defluorination, which indicates that •OH does not play a key role in the rate-determining steps of the photochemical degradation of PFOA.

#### 4. Conclusions

In this study, a novel, efficient degradation approach of PFOA under UV-A irradiation after adsorption on Fe-zeolites with molecular oxygen being the terminal oxidant was established. Experimental results show i) Fe-zeolites based photochemical system exhibits a better PFOA degradation performance under irradiation (a wider range from UV-C to UV-A) compared to the homogeneous ferric ions system. ii) Slightly acidic conditions are optimal in terms of PFOA adsorption and complexation. iii) Molecular oxygen works as the terminal oxidant and is involved in re-oxidization of ferrous ions to ferric ions, producing reactive species and facilitating further mineralization of PFOA. iv) Except for SO<sub>4</sub><sup>2-</sup>, the presence of other commonly present inorganic anions has a negligible impact on PFOA degradation. v) The isolated Fe<sup>3+</sup> ions in octahedral coordination are involved in the carboxylate-to-metal charge transfer, which plays the major role

in the process of PFOA degradation. Using Fe-zeolites as both adsorbent and photocatalyst opens up the design of new technological approaches for degradation of PFOA. A feasible process scheme could consist of the following steps: in the first step, PFOA is removed from water by adsorption to the Fe-zeolites that can then be separated by microfiltration. In the second step, the loaded zeolite particles can be regenerated *in situ* by photochemical degradation under optimal reaction conditions with UV-A irradiation ( $300 \text{ nm} < \lambda < 400 \text{ nm}$ ), i.e. a solar light fraction. Post-treatment of the regeneration solution by UV-C/persulfate can be used for complete mineralization of released shorter-chain PFCAs. Overall, a combination of PFOA adsorptive enrichment and photochemical degradation by applying Fe-zeolites can be realized, which is promising for the treatment of this highly recalcitrant trace-level contaminant.

## **Acknowledgments**

We thank Mireia Arqué Hernández for technical support in experimental design, Dr. Roberto Köferstein (Martin-Luther-Universität Halle-Wittenberg, Germany) for the XRD analysis. L.Q. acknowledges financial support by China Scholarship Council.

**Table 1.** Adsorbed fraction ( $X_{\text{sorb}}$ , in %) and loading of PFOA on zeolite (in  $\text{mg g}^{-1}$ ) after 24 h shaking at various initial pH values in aqueous suspension.  $C_{0,\text{PFOA}} = 48 \mu\text{M}$  and  $C_{\text{Fe-BEA35}} = 1 \text{ g L}^{-1}$

	pH = 3.0	pH = 5.5	pH = 7.0	pH = 9.0
$X_{\text{sorb}}$ (%)	98	84	68	66
Loading of PFOA on zeolite ( $\text{mg g}^{-1}$ )	20	17	14	13

**Table 2.** Defluorination ratios ( $d_{\text{F}^-}$ ), pseudo-first-order degradation rate constants ( $k_{\text{obs,PFOA}}$ ) for initial reaction period (6 h) and half-lives of PFOA degradation with Fe-BEA35 and UV-A irradiation under various reaction conditions.  $C_{0,\text{PFOA}} = 48 \mu\text{M}$  and  $C_{\text{Fe-BEA35}} = 1 \text{ g L}^{-1}$ , inorganic salts were added (only where stated) at a concentration of 10 mM.

	pH = 3.0 <sup>a</sup>	pH = 5.5 <sup>a</sup>	pH = 7.0 <sup>a</sup>	pH = 9.0 <sup>a</sup>	N <sub>2</sub> <sup>b</sup>	Na <sub>2</sub> SO <sub>4</sub> <sup>c</sup>	NaCl <sup>c</sup>	NaClO <sub>4</sub> <sup>c</sup>	NaNO <sub>3</sub> <sup>c</sup>
$d_{\text{F}^-}$ after 24 h (%)	39 ± 1 <sup>d</sup>	38 ± 1	5.5 ± 0.2	1.1 ± 0.1	12.0 ± 0.5	28 ± 1	32 ± 1	36 ± 1	33 ± 1
$k_{\text{obs,PFOA}}$ (h <sup>-1</sup> )	0.44 ± 0.02	0.38 ± 0.04	0.019 ± 0.005	0.011 ± 0.007	0.059 ± 0.016	0.063 ± 0.007	0.32 ± 0.06	0.35 ± 0.08	0.39 ± 0.10
PFOA $t_{1/2}$ (h)	1.6 ± 0.1	1.8 ± 0.2	37 ± 8	63 ± 25	12 ± 2	11 ± 1	2.2 ± 0.3	2.0 ± 0.4	1.8 ± 0.4

<sup>a</sup> The suspensions were initially purged with oxygen. pH values are initial values.

<sup>b</sup> The initial pH of suspension was 5.5 and the suspension was initially purged with N<sub>2</sub>.

<sup>c</sup> The suspensions were initially purged with oxygen. The initial pH of suspensions was 5.5.  $C_{\text{salt}} = 10 \text{ mM}$

<sup>d</sup> Error ranges represent average deviations of single values from the mean of triplicate assays.

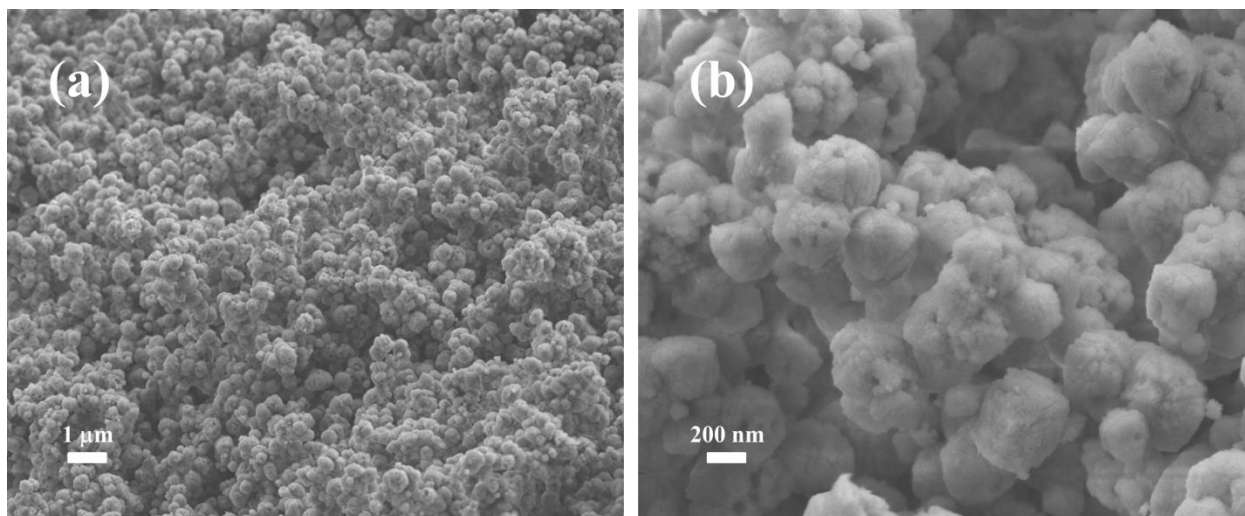


**Figure 1.** Scanning electron microscope (SEM) images of Fe-BEA35.

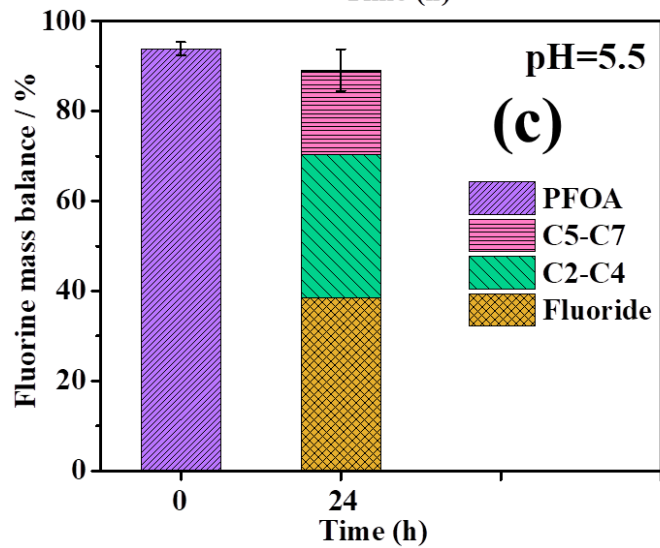
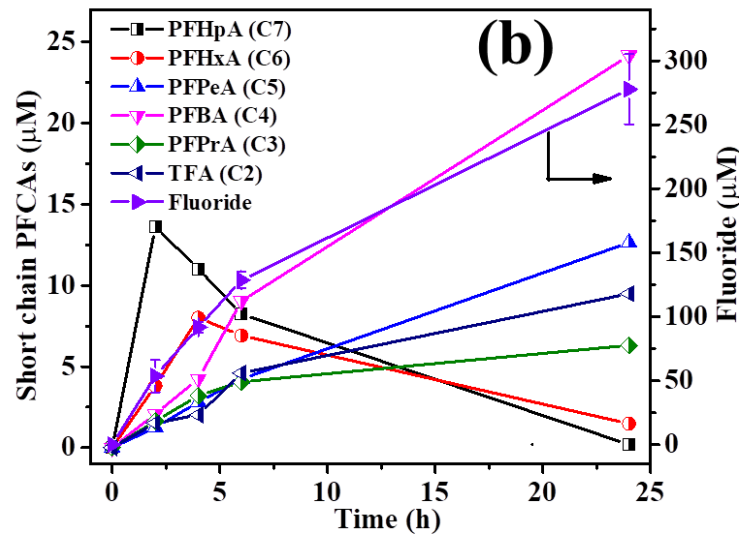
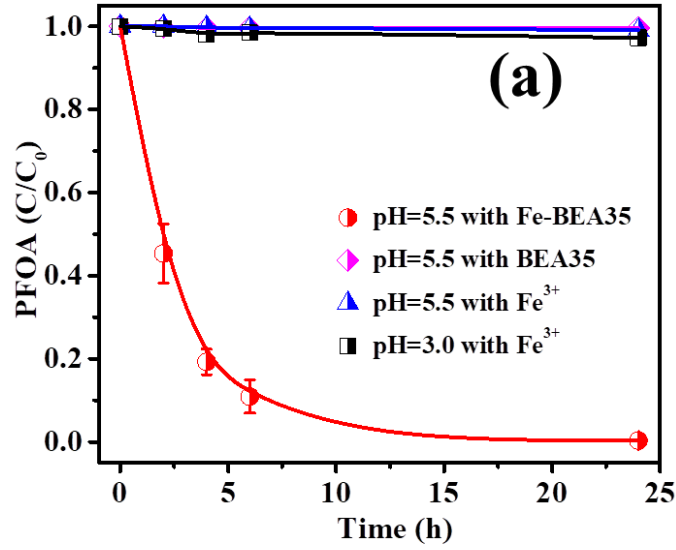


**Figure 2.** Degradation of PFOA under UV-A irradiation ( $C_{0,\text{PFOA}} = 48 \mu\text{M}$ , oxygen atmosphere,  $1 \text{ g L}^{-1}$  (Fe-)BEA35 and  $C_{0,\text{Fe}^{3+}} = 200 \mu\text{M}$ , where applied). (a) Comparison of degradation in presence of ferric ions, Fe-BEA35 and BEA35 ( $\text{pH}_0 = 3$  and  $\text{pH}_0 = 5.5$ ). (b) Formation of short-chain intermediates and fluoride in the presence of Fe-BEA35 ( $1 \text{ g L}^{-1}$ ,  $\text{pH}_0 = 5.5$ ). (c) Mass balance of fluorine for the above experiment. Mass balance at 0 h represents F detected as PFOA in ACN extract of zeolite suspension before start of reaction, and at 24 h is composed of fluorine detected as C2-C4 PFCAs and fluoride in aqueous phase of suspension as well as C5 to C7 PFCAs in ACN extract of suspension. Error ranges represent average deviations of single values from the mean of triplicate assays in Figures 1(a) and (b). Error bars for individual PFCAs were omitted for the sake of clarity but are exemplarily shown for PFPeA. The cumulative error is shown in Figure 1(c). Lines are added to guide the eye.

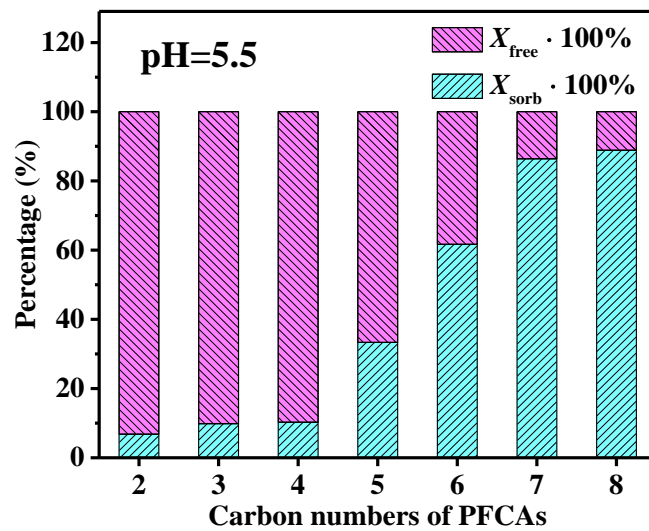


**Figure 3.** Results of adsorption experiments: distribution of PFCAs with various chain lengths between zeolite Fe-BEA35 ( $X_{\text{sorb}}$ ) and the aqueous phase ( $X_{\text{free}}$ ) after 4 days shaking.  $C_{\text{Fe-BEA35}} = 1 \text{ g L}^{-1}$ ,  $C_{0,\text{PFCAs}} = 48 \text{ }\mu\text{M}$  and  $\text{pH}_0 = 5.5$ .

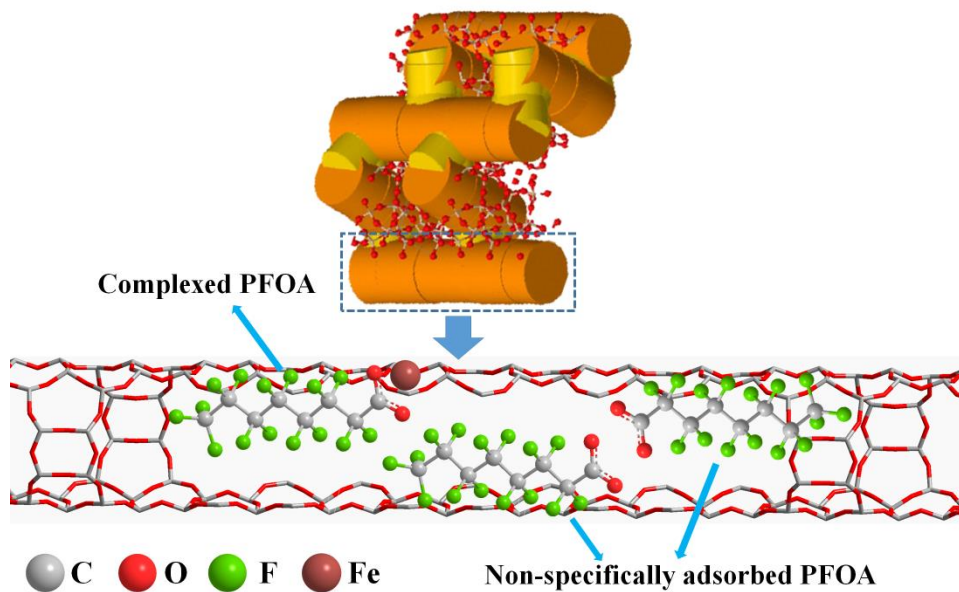


**Figure 4.** Scheme of PFOA configurations on Fe-BEA35 with and without specific adsorption. Up: Cutaway of BEA framework with 2-1-1 unit cells; Down: Zoom-in of a single channel. The complexed PFOA means the specifically adsorbed PFOA at ferric ions.

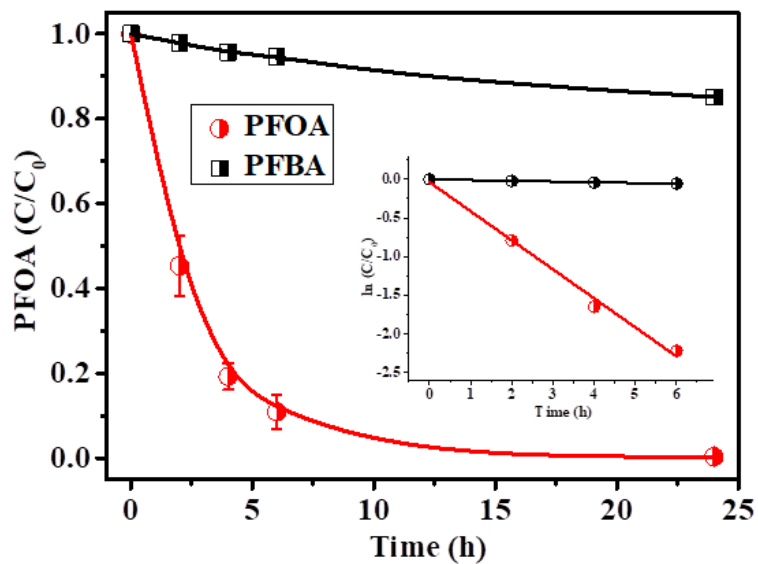


**Figure 5.** The comparison of PFOA and PFBA degradation in the presence of Fe-BEA35 ( $1 \text{ g L}^{-1}$ ) under UV-A irradiation.  $C_{0,\text{PFCAs}} = 48 \text{ } \mu\text{M}$ ,  $\text{pH}_0 = 5.5$ , oxygen atmosphere. Error bars represent standard deviations of triplicate assays. Lines are added to guide the eye.

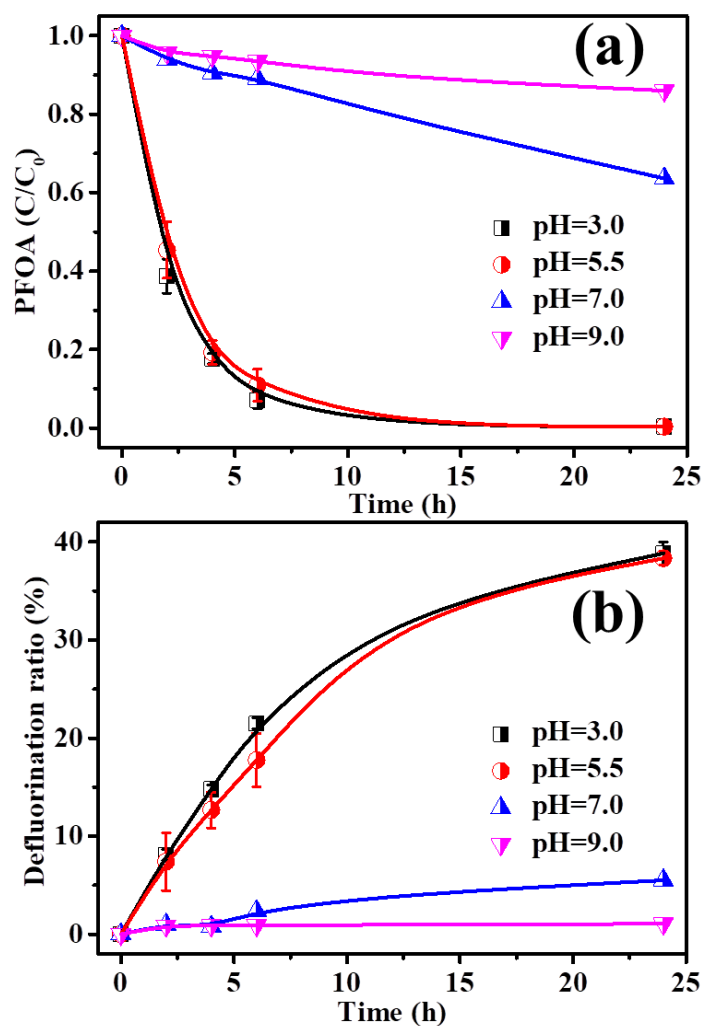


**Figure 6.** Degradation of PFOA under UV-A irradiation in the presence of Fe-BEA35 (1 g L<sup>-1</sup>) at various initial pH values. Time course of (a) residual PFOA concentration and (b) defluorination ratios ( $d_{F^-}$ ).  $C_{0,PFOA} = 48 \mu\text{M}$ , oxygen atmosphere. Error ranges represent average deviations of single values from the mean of triplicate assays. Lines are added to guide the eye.

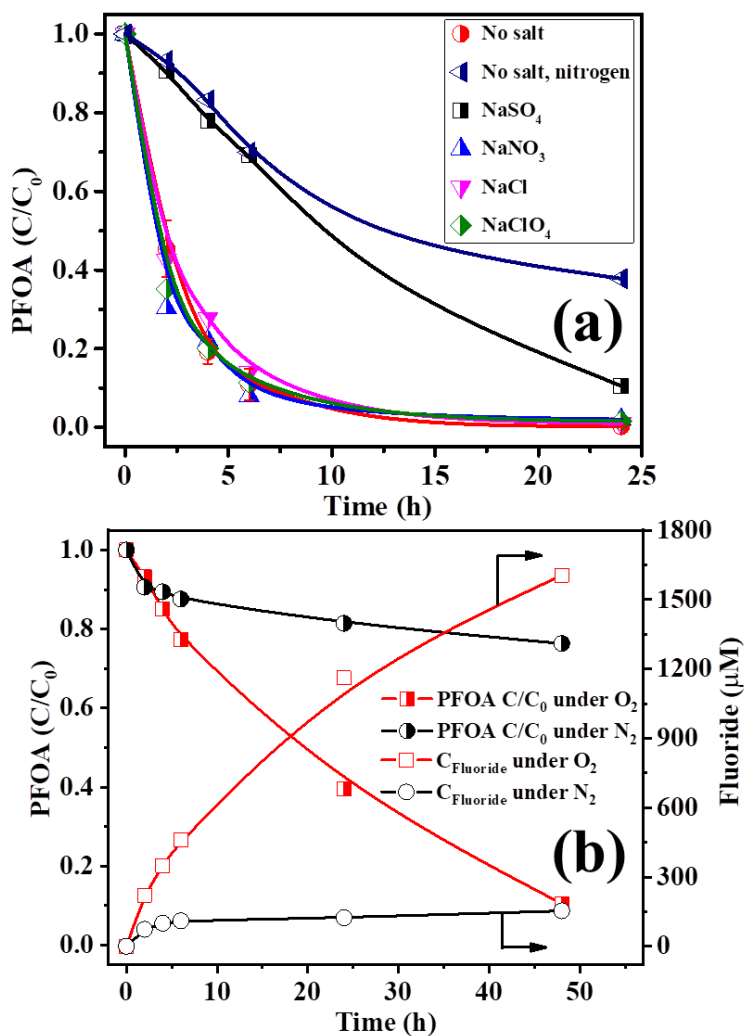


**Figure 7.** Effect of inorganic ions and gas atmosphere on photochemical degradation of PFOA in the presence of Fe-zeolite under UV-A light.  $C_{0,PFOA} = 48 \mu\text{M}$  or  $480 \mu\text{M}$ ,  $1 \text{ g L}^{-1}$  Fe-BEA35,  $10 \text{ mM SO}_4^{2-}$ ,  $\text{Cl}^-$ ,  $\text{NO}_3^-$ , and  $\text{ClO}_4^-$  were added where applied,  $\text{pH}_0 = 5.5$  and oxygen atmosphere where not otherwise stated. (a) Influence of inorganic ions and atmosphere at  $C_{0,PFOA} = 48 \mu\text{M}$ . (b) Influence of atmosphere ( $\text{O}_2$  or  $\text{N}_2$ ) at  $C_{0,PFOA} = 480 \mu\text{M}$ . Lines are added to guide the eye.

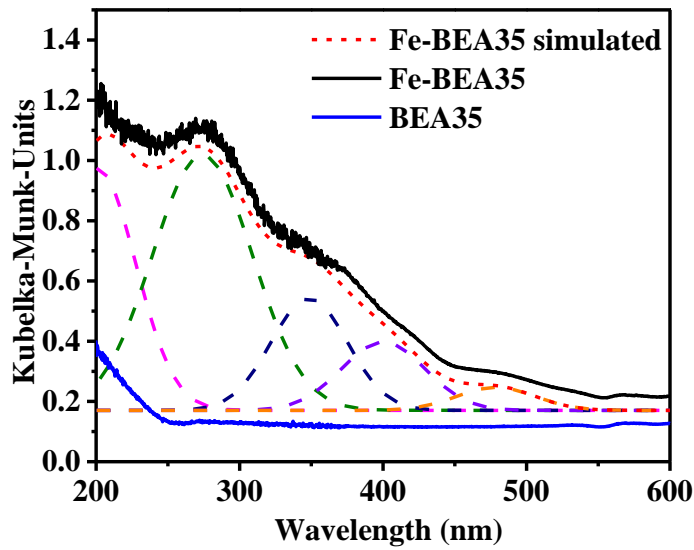


**Figure 8.** UV-vis-DR spectra of  $10 \text{ g L}^{-1}$  Fe-BEA35 suspension (black line) and  $10 \text{ g L}^{-1}$  BEA35 suspension (blue line), simulated deconvolution curves for UV-vis-DR spectra of Fe-BEA35 suspension (dashed lines).

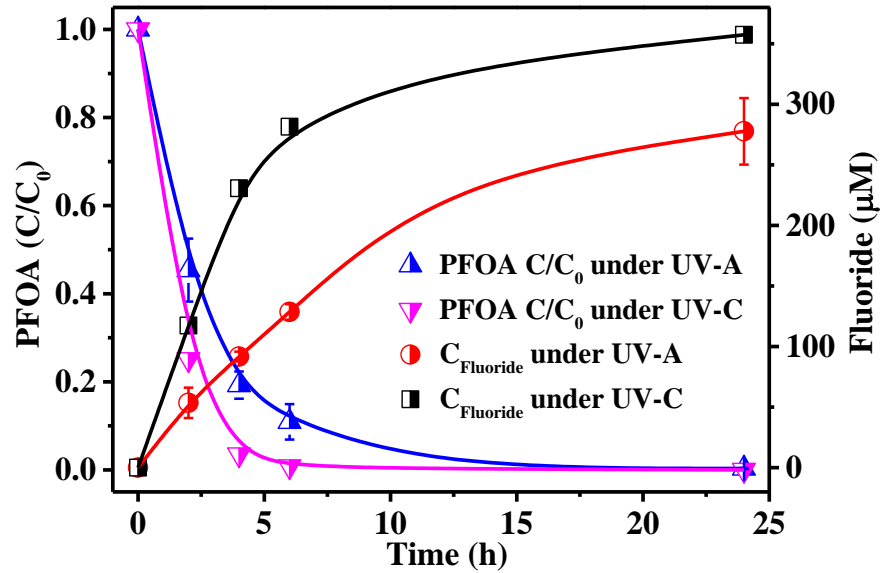


**Figure 9.** Degradation of PFOA in the presence of Fe-BEA35 ( $1 \text{ g L}^{-1}$ ) under UV-A and UV-C irradiation.  $C_{0,\text{PFOA}} = 48 \text{ } \mu\text{M}$ ,  $\text{pH}_0 = 5.5$ , oxygen atmosphere. Error bars represent standard deviations of triplicate assays. Lines are added to guide the eye.

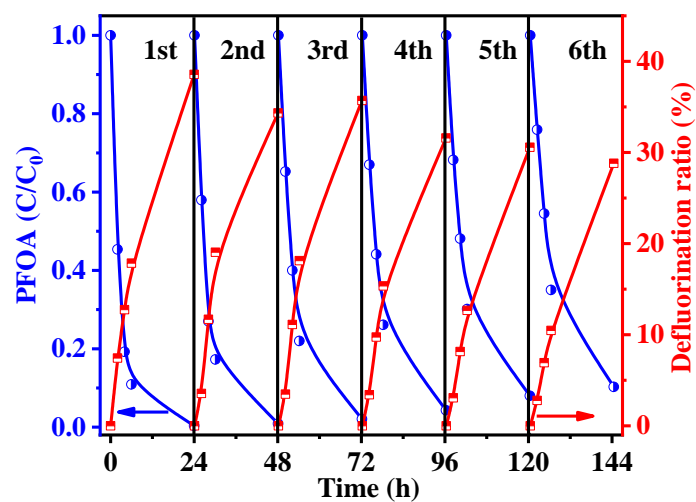
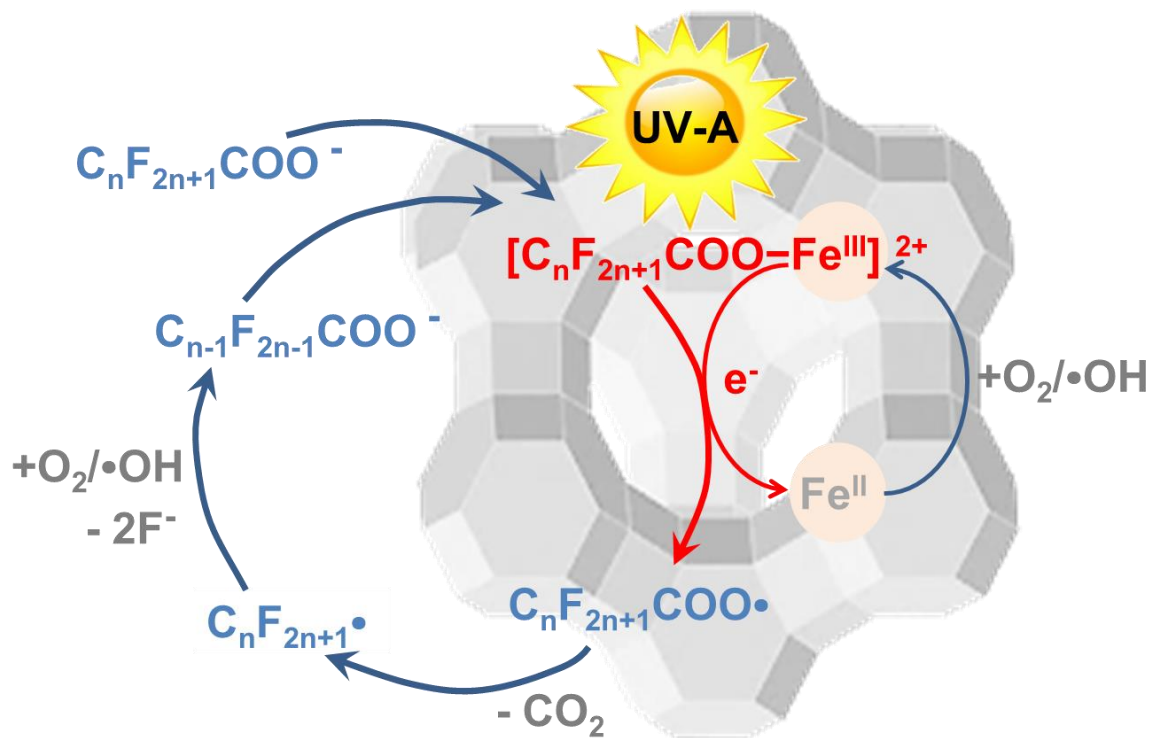


**Figure 10.** PFOA degradation and defluorination in consecutive batch runs with Fe-BEA35 (1 g L<sup>-1</sup>) under UV-A light.  $C_{0,\text{PFOA}} = 48 \mu\text{M}$  each,  $\text{pH}_0 = 5.5$ , oxygen atmosphere. Lines are added to guide the eye.



**Scheme 1.** Hypothetical reaction mechanism for the photochemical degradation of PFOA on Fe-BEA35.

## References

- [1] H.-J. Lehmler, Synthesis of environmentally relevant fluorinated surfactants - a review, *Chemosphere* 58 (2005) 1471-1496. <https://doi.org/10.1016/j.chemosphere.2004.11.078>
- [2] A.B. Lindstrom, M.J. Strynar, E.L. Libelo, Polyfluorinated compounds: Past, present, and future, *Environ. Sci. Technol.* 45 (2011) 7954-7961. <https://doi.org/10.1021/es2011622>
- [3] C. Baduel, C.J. Paxman, J.F. Mueller, Perfluoroalkyl substances in a firefighting training ground (FTG), distribution and potential future release, *J. Hazard. Mater.* 296 (2015) 46-53. <https://doi.org/10.1016/j.jhazmat.2015.03.007>
- [4] C.A. Moody, J.A. Field, Perfluorinated surfactants and the environmental implications of their use in fire-fighting foams, *Environ. Sci. Technol.* 34 (2000) 3864-3870. <https://doi.org/10.1021/es991359u>
- [5] C.P. Higgins, R.G. Luthy, Sorption of perfluorinated surfactants on sediments, *Environ. Sci. Technol.* 40 (2006) 7251-7256. <https://doi.org/10.1021/es061000n>
- [6] J.A. Björklund, K. Thuresson, C.A. De Wit, Perfluoroalkyl compounds (PFCs) in indoor dust: concentrations, human exposure estimates, and sources, *Environ. Sci. Technol.* 43 (2009) 2276-2281. <https://doi.org/10.1021/es803201a>
- [7] J. Hollingsworth, R. Sierra-Alvarez, M. Zhou, K.L. Ogden, J.A. Field, Anaerobic biodegradability and methanogenic toxicity of key constituents in copper chemical mechanical planarization effluents of the semiconductor industry, *Chemosphere* 59 (2005) 1219-1228. <https://doi.org/10.1016/j.chemosphere.2004.11.067>
- [8] B.D. Key, R.D. Howell, C.S. Criddle, Fluorinated organics in the biosphere, *Environ. Sci. Technol.* 31 (1997) 2445-2454. <https://doi.org/10.1021/es961007c>
- [9] M.M. Schultz, C.P. Higgins, C.A. Huset, R.G. Luthy, D.F. Barofsky, J.A. Field, Fluorochemical mass flows in a municipal wastewater treatment facility, *Environ. Sci. Technol.* 40 (2006) 7350-7357. <https://doi.org/10.1021/es061025m>
- [10] C.K.O. da Silva-Rackov, W.A. Lawal, P.A. Nfodzo, M. Vianna, C.A.O. do Nascimento, H. Choi, Degradation of PFOA by hydrogen peroxide and persulfate activated by iron-modified diatomite, *Appl. Catal. B Environ.* 192 (2016) 253-259. <https://doi.org/10.1016/j.apcatb.2016.03.067>
- [11] K.H. Kucharzyk, R. Darlington, M. Benotti, R. Deeb, E. Hawley, Novel treatment technologies for PFAS compounds: A critical review, *Journal of environmental management* 204 (2017) 757-764. <https://doi.org/10.1016/j.jenvman.2017.08.016>
- [12] H. Park, C.D. Vecitis, J. Cheng, N.F. Dalleska, B.T. Mader, M.R. Hoffmann, Reductive degradation of perfluoroalkyl compounds with aquated electrons generated from iodide photolysis at 254 nm, *Photochem. Photobiol. Sci.* 10 (2011) 1945-1953. <https://doi.org/10.1039/C1PP05270E>
- [13] H. Hori, A. Yamamoto, K. Koike, S. Kutsuna, M. Murayama, A. Yoshimoto, R. Arakawa, Photocatalytic decomposition of a perfluoroether carboxylic acid by tungstic heteropolyacids in water, *Appl. Catal. B Environ.* 82 (2008) 58-66. <https://doi.org/10.1016/j.apcatb.2008.01.031>
- [14] H. Zhao, J. Gao, G. Zhao, J. Fan, Y. Wang, Y. Wang, Fabrication of novel SnO<sub>2</sub>-Sb/carbon aerogel electrode for ultrasonic electrochemical oxidation of perfluorooctanoate with high catalytic efficiency, *Appl. Catal. B Environ.* 136 (2013) 278-286. <https://doi.org/10.1016/j.apcatb.2013.02.013>

- [15] Q. Zhuo, S. Deng, B. Yang, J. Huang, G. Yu, Efficient electrochemical oxidation of perfluorooctanoate using a Ti/SnO<sub>2</sub>-Sb-Bi anode, *Environ. Sci. Technol.* 45 (2011) 2973-2979. <https://doi.org/10.1021/es1024542>
- [16] Z. Li, P. Zhang, T. Shao, X. Li, In<sub>2</sub>O<sub>3</sub> nanoporous nanosphere: a highly efficient photocatalyst for decomposition of perfluorooctanoic acid, *Appl. Catal. B Environ.* 125 (2012) 350-357. <https://doi.org/10.1016/j.apcatb.2012.06.017>
- [17] H. Hori, A. Yamamoto, E. Hayakawa, S. Taniyasu, N. Yamashita, S. Kutsuna, H. Kiatagawa, R. Arakawa, Efficient decomposition of environmentally persistent perfluorocarboxylic acids by use of persulfate as a photochemical oxidant, *Environ. Sci. Technol.* 39 (2005) 2383-2388. <https://doi.org/10.1021/es0484754>
- [18] H. Hori, Y. Nagaoka, M. Murayama, S. Kutsuna, Efficient decomposition of perfluorocarboxylic acids and alternative fluorochemical surfactants in hot water, *Environ. Sci. Technol.* 42 (2008) 7438-7443. <https://doi.org/10.1021/es800832p>
- [19] H.V. Lutze, J. Brekenfeld, S. Naumov, C. von Sonntag, T.C. Schmidt, Degradation of perfluorinated compounds by sulfate radicals—New mechanistic aspects and economical considerations, *Water Res.* 129 (2018) 509-519. <https://doi.org/10.1016/j.watres.2017.10.067>
- [20] Y. Wang, P. Zhang, G. Pan, H. Chen, Ferric ion mediated photochemical decomposition of perfluorooctanoic acid (PFOA) by 254 nm UV light, *J. Hazard. Mater.* 160 (2008) 181-186. <https://doi.org/10.1016/j.jhazmat.2008.02.105>
- [21] Y. Qu, C. Zhang, F. Li, J. Chen, Q. Zhou, Photo-reductive defluorination of perfluorooctanoic acid in water, *Water Res.* 44 (2010) 2939-2947. <https://doi.org/10.1016/j.watres.2010.02.019>
- [22] H. Tang, Q. Xiang, M. Lei, J. Yan, L. Zhu, J. Zou, Efficient degradation of perfluorooctanoic acid by UV–Fenton process, *Chem. Eng. J.* 184 (2012) 156-162. <https://doi.org/10.1016/j.cej.2012.01.020>
- [23] H. Hori, A. Yamamoto, K. Koike, S. Kutsuna, I. Osaka, R. Arakawa, Photochemical decomposition of environmentally persistent short-chain perfluorocarboxylic acids in water mediated by iron (II)/(III) redox reactions, *Chemosphere* 68 (2007) 572-578. <https://doi.org/10.1016/j.chemosphere.2006.12.038>
- [24] J.-h. Cheng, X.-y. Liang, S.-w. Yang, Y.-y. Hu, Photochemical defluorination of aqueous perfluorooctanoic acid (PFOA) by VUV/Fe<sup>3+</sup> system, *Chem. Eng. J.* 239 (2014) 242-249. <https://doi.org/10.1016/j.cej.2013.11.023>
- [25] L. Jin, P. Zhang, T. Shao, S. Zhao, Ferric ion mediated photodecomposition of aqueous perfluorooctane sulfonate (PFOS) under UV irradiation and its mechanism, *J. Hazard. Mater.* 271 (2014) 9-15. <https://doi.org/10.1016/j.jhazmat.2014.01.061>
- [26] S. Navalon, M. Alvaro, H. Garcia, Heterogeneous Fenton catalysts based on clays, silicas and zeolites, *Appl. Catal. B Environ.* 99 (2010) 1-26. <https://doi.org/10.1016/j.apcatb.2010.07.006>
- [27] M. Hartmann, S. Kullmann, H. Keller, Wastewater treatment with heterogeneous Fenton-type catalysts based on porous materials, *J. Mater. Chem.* 20 (2010) 9002-9017. <https://doi.org/10.1039/C0JM00577K>
- [28] R. Gonzalez-Olmos, F.-D. Kopinke, K. Mackenzie, A. Georgi, Hydrophobic Fe-zeolites for removal of MTBE from water by combination of adsorption and oxidation, *Environ. Sci. Technol.* 47 (2013) 2353-2360. <https://doi.org/10.1021/es303885y>

- [29] A. Zecchina, M. Rivallan, G. Berlier, C. Lamberti, G. Ricchiardi, Structure and nuclearity of active sites in Fe-zeolites: comparison with iron sites in enzymes and homogeneous catalysts, *Phys. Chem. Chem. Phys.* 9 (2007) 3483-3499. <https://doi.org/10.1039/B703445H>
- [30] R. Gonzalez-Olmos, M.J. Martin, A. Georgi, F.-D. Kopinke, I. Oller, S. Malato, Fe-zeolites as heterogeneous catalysts in solar Fenton-like reactions at neutral pH, *Appl. Catal. B Environ.* 125 (2012) 51-58. <https://doi.org/10.1016/j.apcatb.2012.05.022>
- [31] G. Gillies, R. Raj, F.-D. Kopinke, A. Georgi, Suspension stability and mobility of Trap-Ox Fe-zeolites for in-situ nanoremediation, *J. Colloid Interface Sci.* 501 (2017) 311-320. <https://doi.org/10.1016/j.jcis.2017.04.037>
- [32] A.L. Allred, Electronegativity values from thermochemical data, *J. Inorg. Nuclear Chem.* 17 (1961) 215-221. [https://doi.org/10.1016/0022-1902\(61\)80142-5](https://doi.org/10.1016/0022-1902(61)80142-5)
- [33] Database of Zeolite Structures., [http://www.iza-structure.org/IZA-SC/framework\\_3d.php?STC=BEA](http://www.iza-structure.org/IZA-SC/framework_3d.php?STC=BEA)
- [34] R. Gonzalez-Olmos, U. Roland, H. Toufar, F.-D. Kopinke, A. Georgi, Fe-zeolites as catalysts for chemical oxidation of MTBE in water with H<sub>2</sub>O<sub>2</sub>, *Appl. Catal. B Environ.* 89 (2009) 356-364. <https://doi.org/10.1016/j.apcatb.2008.12.014>
- [35] L. Čapek, V. Kreibich, J. Dědeček, T. Grygar, B. Wichterlova, Z. Sobalik, J. Martens, R. Brosius, V. Tokarova, Analysis of Fe species in zeolites by UV–VIS–NIR, IR spectra and voltammetry. Effect of preparation, Fe loading and zeolite type, *Micropor. Mesopor. Mater.* 80 (2005) 279-289. <https://doi.org/10.1016/j.micromeso.2004.12.014>
- [36] G.D. Pirngruber, P.K. Roy, R. Prins, On determining the nuclearity of iron sites in Fe-ZSM-5—a critical evaluation, *Phys. Chem. Chem. Phys.* 8 (2006) 3939-3950. <https://doi.org/10.1039/B606205A>
- [37] J.B. Higgins, R.B. LaPierre, J.L. Schlenker, A.C. Rohrman, J.D. Wood, G.T. Kerr, W.J. Rohrbaugh, The framework topology of zeolite beta, *Zeolites* 8 (1988) 446-452. [https://doi.org/10.1016/S0144-2449\(88\)80219-7](https://doi.org/10.1016/S0144-2449(88)80219-7)
- [38] S. Shwan, R. Nedyalkova, J. Jansson, J. Korsgren, L. Olsson, M. Skoglundh, Hydrothermal stability of Fe–BEA as an NH<sub>3</sub>-SCR catalyst, *Industrial & engineering chemistry research* 51 (2012) 12762-12772. <https://doi.org/10.1021/ie301516z>
- [39] A. Hagenaaers, L. Vergauwen, W. De Coen, D. Knapeen, Structure–activity relationship assessment of four perfluorinated chemicals using a prolonged zebrafish early life stage test, *Chemosphere* 82 (2011) 764-772. <https://doi.org/10.1016/j.chemosphere.2010.10.076>
- [40] M.-J. Lopez-Espinosa, T. Fletcher, B. Armstrong, B. Genser, K. Dhatariya, D. Mondal, A. Ducatman, G. Leonardi, Association of perfluorooctanoic acid (PFOA) and perfluorooctane sulfonate (PFOS) with age of puberty among children living near a chemical plant, *Environmental science & technology* 45 (2011) 8160-8166. <https://doi.org/10.1021/es1038694>
- [41] K. Kleszczyński, A.C. Składanowski, Mechanism of cytotoxic action of perfluorinated acids. III. Disturbance in Ca<sup>2+</sup> homeostasis, *Toxicology and applied pharmacology* 251 (2011) 163-168. <https://doi.org/10.1016/j.taap.2011.01.002>
- [42] U. Shafique, V. Dorn, A. Paschke, G. Schuurmann, Adsorption of perfluorocarboxylic acids at the silica surface, *Chem. Commun.* 53 (2017) 589-592. <https://doi.org/10.1039/c6cc07525h>
- [43] K.-U. Goss, The pK<sub>a</sub> Values of PFOA and other highly fluorinated carboxylic acids, *Environ. Sci. Technol.* 42 (2008) 456-458. <https://doi.org/10.1021/es702192c>
- [44] E. Hogfeldt, Stability constants of metal-ion complexes. Part A Inorganic ligands. International Union of Pure and Applied Chemists., Pergamon Press, New York, 1982.

- [45] H.J. Benkelberg, P. Warneck, Photodecomposition of iron(III) hydroxo and sulfato complexes in aqueous solution: Wavelength dependence of OH and SO<sub>4</sub>-quantum yields, *J. Phys. Chem.* 99 (1995) 5214-5221. <https://doi.org/10.1021/j100014a049>
- [46] M. Schwidder, M.S. Kumar, K. Klementiev, M.M. Pohl, A. Bruckner, W. Gruenert, Selective reduction of NO with Fe-ZSM-5 catalysts of low Fe content - I. Relations between active site structure and catalytic performance, *J. Catal.* 231 (2005) 314-330. <https://doi.org/10.1016/j.jcat.2005.01.031>
- [47] S. Kutsuna, H. Hori, Rate constants for aqueous-phase reactions of SO<sub>4</sub>- with C<sub>2</sub>F<sub>5</sub>C(O)O- and C<sub>3</sub>F<sub>7</sub>C(O)O- at 298 K, *Int. J. Chem. Kinet.* 39 (2007) 276-288. <https://doi.org/10.1002/kin.20239>
- [48] D.V. Avila, K.U. Ingold, J. Lusztyk, W.R. Dolbier, H.Q. Pan, M. Muir, Absolute rate constants for some reactions of perfluoro-n-alkyl radicals in solution, *J. Am. Chem. Soc.* 116 (1994) 99-104. <https://doi.org/10.1021/ja00080a012>